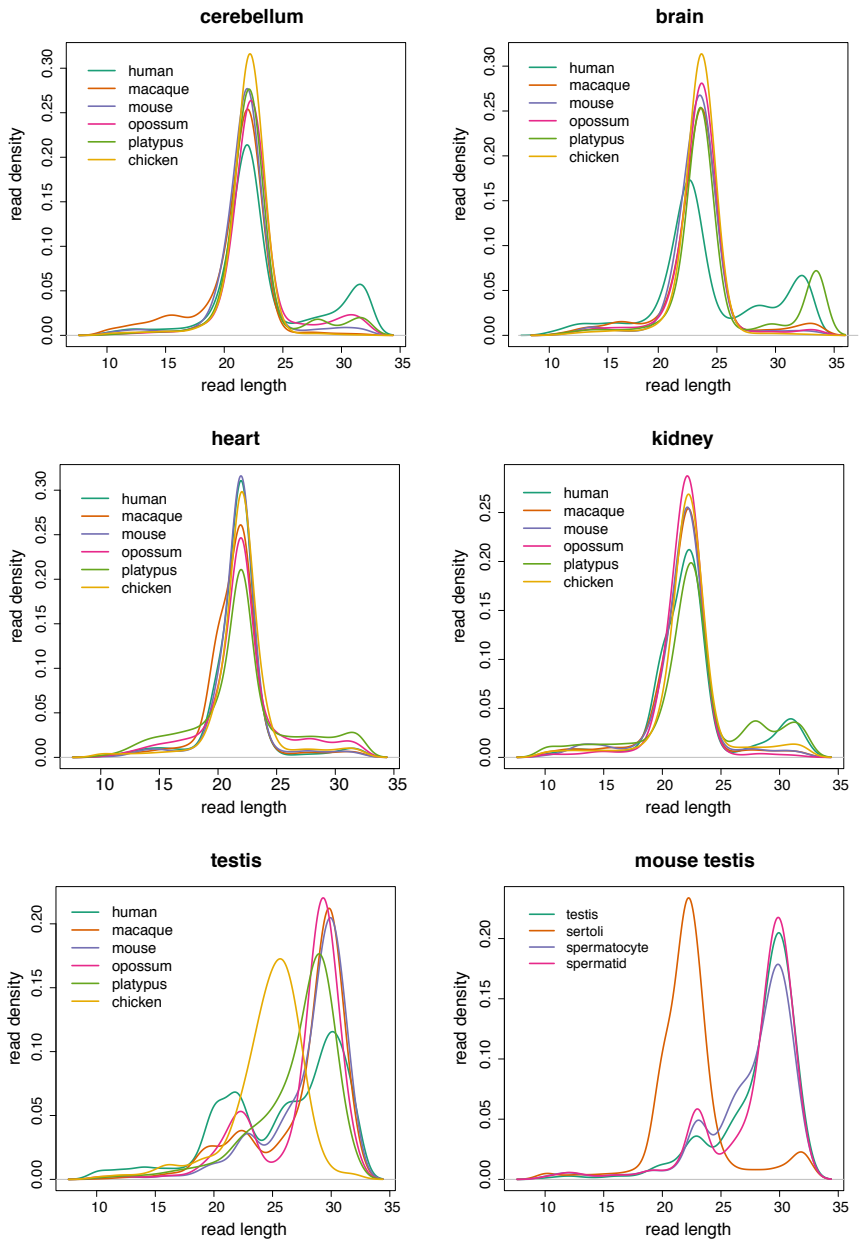

Supplementary Figure 1: read length distribution in small RNA libraries.

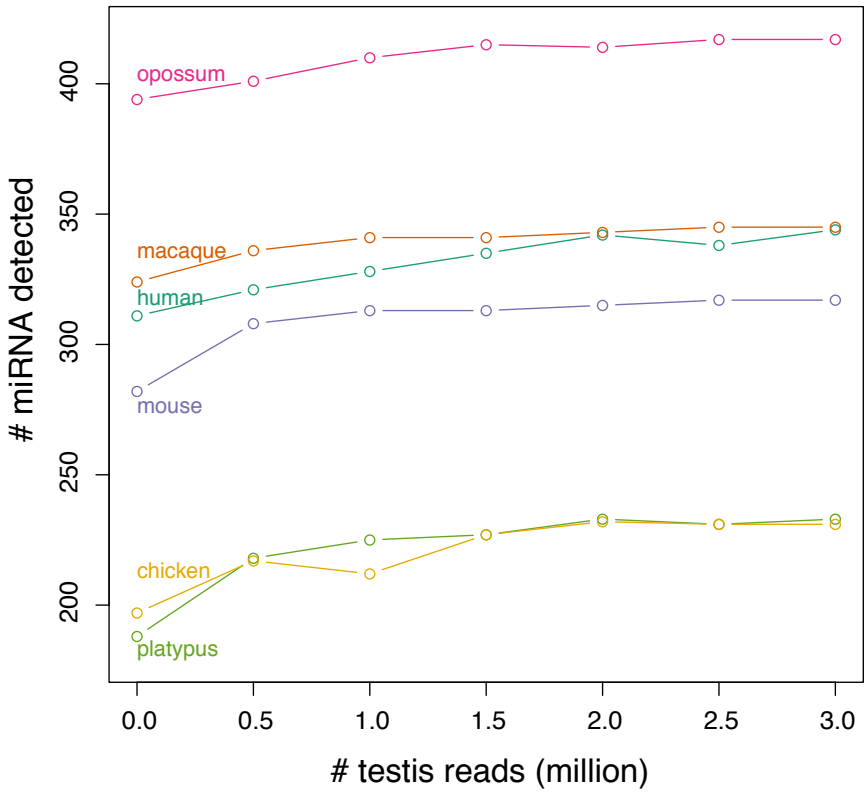

Supplementary Figure 2: Detection of microRNAs and number of testis reads. Number of miRNAs detected by running miRDeep (Methods) using 11 million reads randomly sampled from each somatic tissue and adding a variable amount (0-3 million) of reads randomly sampled from the testis.

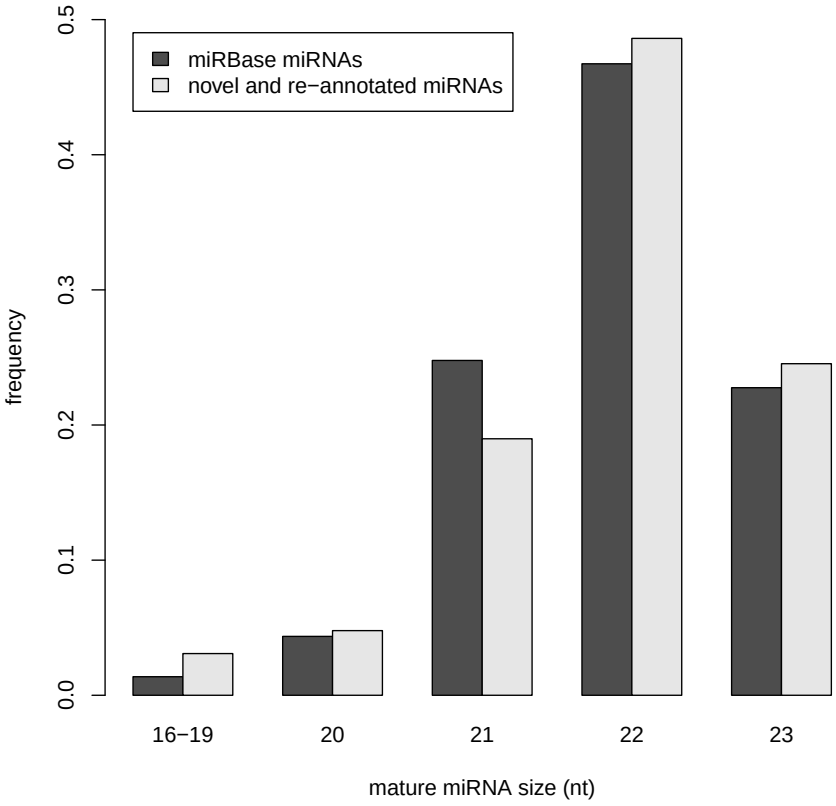

Supplementary Figure 3: Size distribution of mature miRNAs. MiRBase miRNAs: miRNAs in our dataset that are also present in miRBase (Release 15); novel and re-annotated miRNAs: miRNAs in our dataset that are not present in miRBase or re-annotated with different mature and star boundaries.

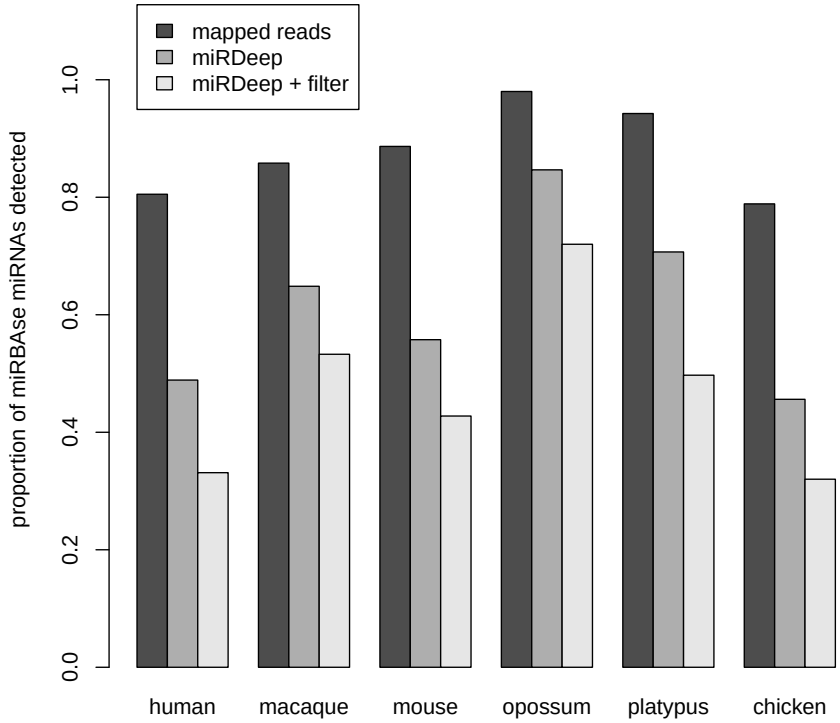

Supplementary Figure 4: Proportion of miRBase miRNAs detected using various methodologies. Mapped reads: miRBase miRNAs (Release 15) with 15-23 nt reads mapping perfectly on the hairpin sequence; miRDeep: miRBase miRNAs overlapping miRNAs predicted by miRDeep; mirDeep + filter: miRBase miRNAs overlapping our miRNA dataset obtained by running miRDeep and filtering its output (Methods).

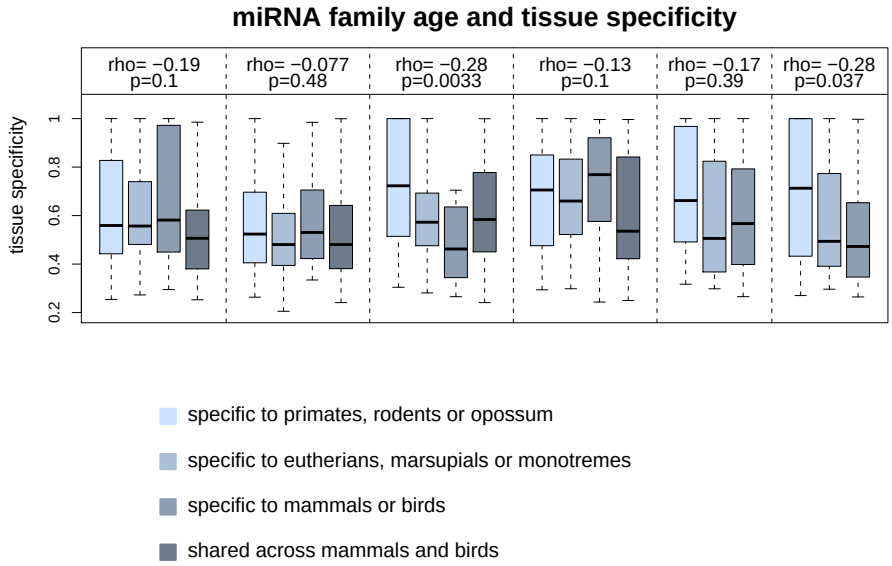

Supplementary Figure 5: Age of miRNA families and tissue specificity. The distributions of tissue specificity values for miRNA families of different ages as assessed by their phylogenetic distributions, are shown. For each miRNA family, we first summed the expression of all family members for each tissue. We then identified in which tissue a miRNA family was the most expressed and divided the expression value in this tissue by the total expression level in all tissues, resulting in an estimate of its tissue specificity. Values supported by less than 30 sequenced reads were discarded from the analysis.

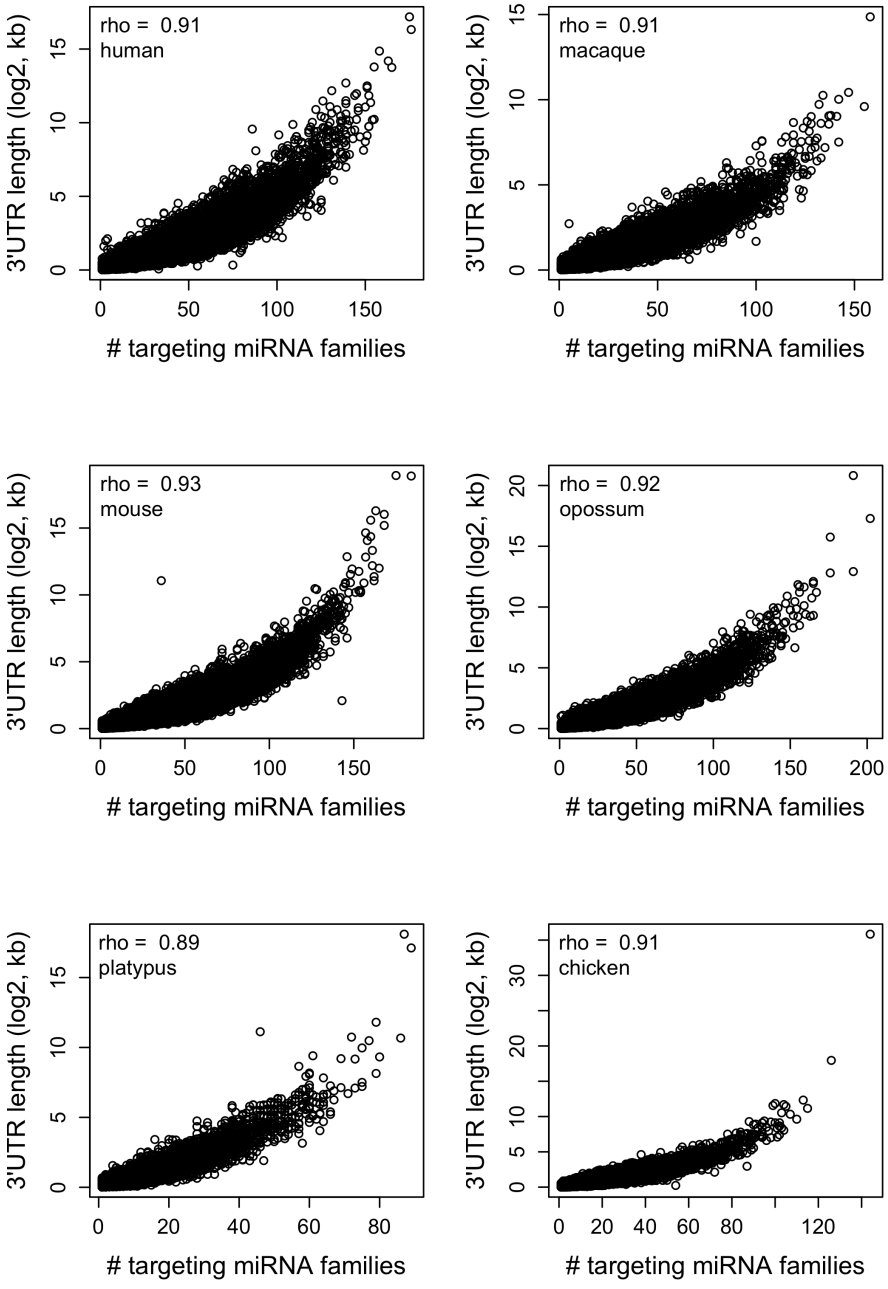

Supplementary Figure 6: Correlation between 3'UTR length and number of targeting miRNA families (PITA). Similar Spearman correlation coefficients were obtained using TargetScan predictions (rho = 0.8-092).

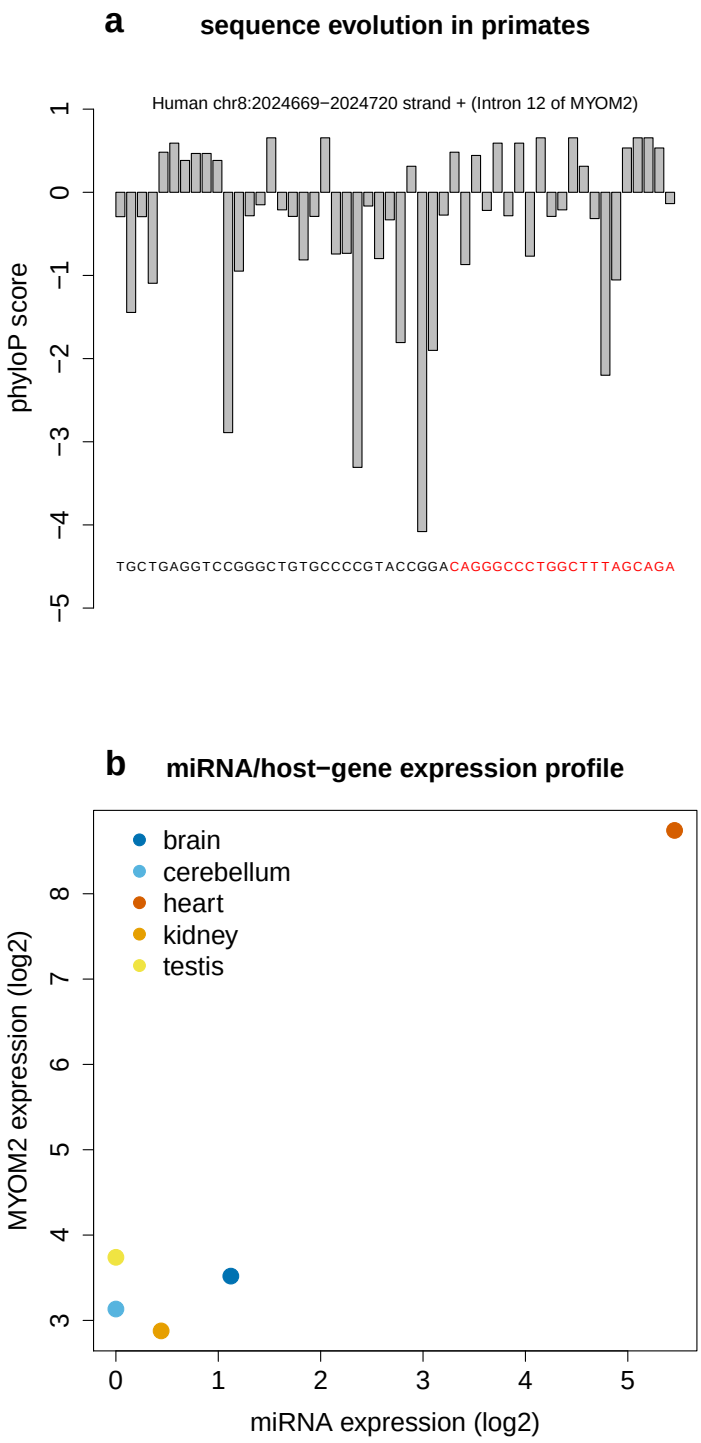

Supplementary Figure 7: Sequence evolution pattern and expression profile of a previously uncharacterized miRNA specific to great apes (hsa-mir-7160). a, PhyloP score distribution for the genomic sequence encoding the precursor sequence. The mature sequence is highlighted in red. The miRNA precursor sequence is located on the sense strand of the intronic sequence of *MYOM2*. **b,** Spatial expression pattern of *MYOM2* and its encoded miRNA.

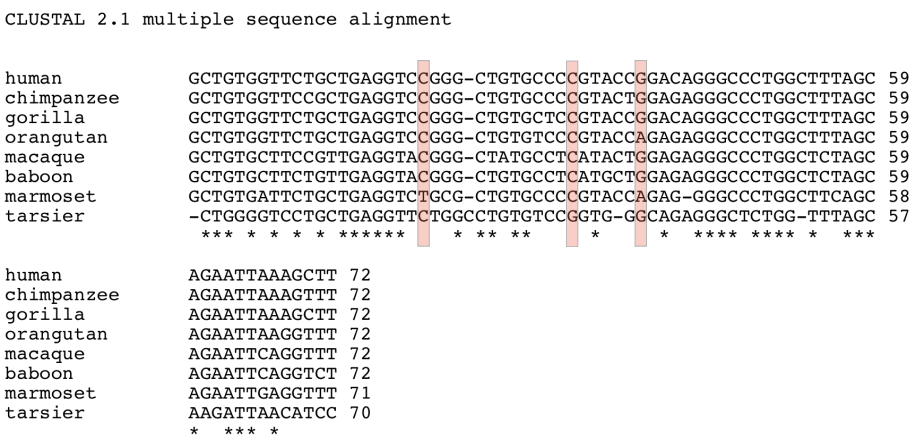

Supplementary Figure 8: Alignment of primate sequences orthologous to the human precursor sequence of a previously uncharacterized miRNA specific to great apes (hsa-mir-7160). The human miRNA precursor sequence (here shown with 10 base pair flanks) is located on the sense strand of the intronic sequence of *MYOM2*. Fast-evolving sites as detected by phyloP are highlighted in red and correspond to hypermutable CpG sites.

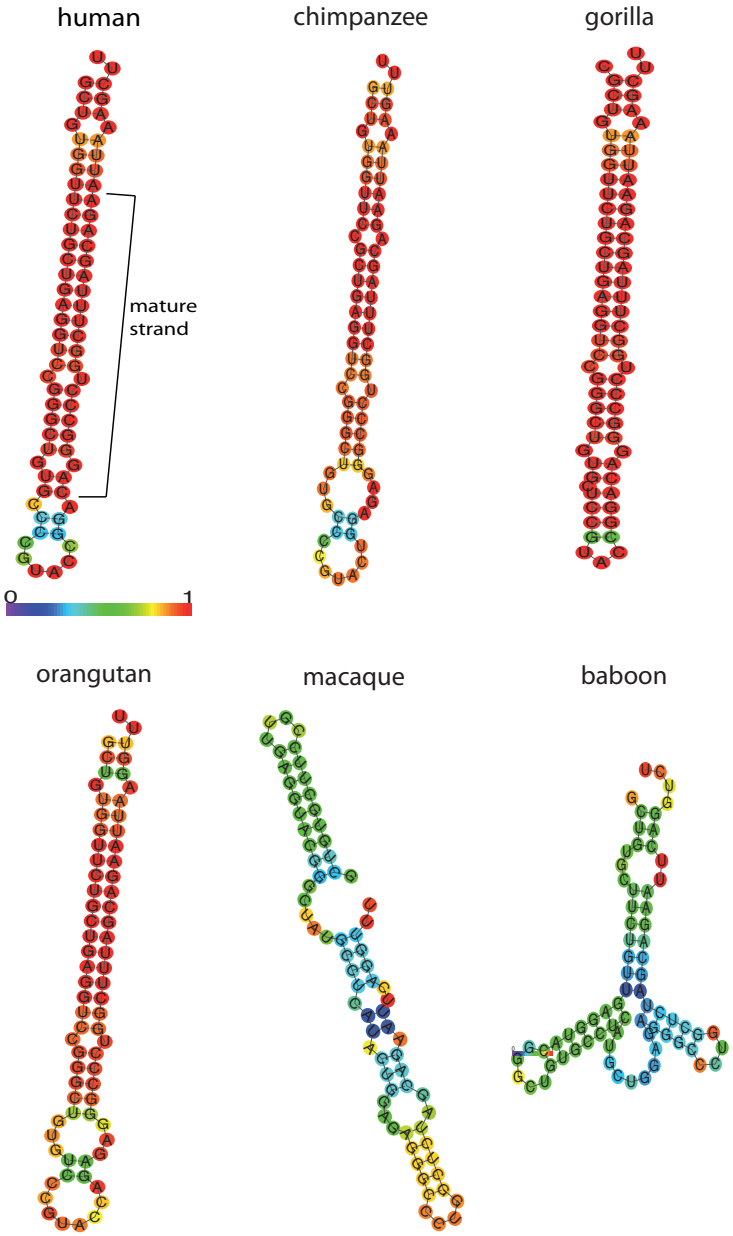

Supplementary Figure 9: Predicted folding structure of the previously uncharacterized intronic MYOM2 miRNA (hsa-mir-7160) and its orthologous sequences across primates. The folding strcutures were predicted by RNAfold (http://rna.tbi.univie.ac.at/cgi-bin/RNAfold.cgi).
Colours indicate pairing probabilities (from 0 in violet to 1 in red). Orthologous sequences in other primates were extracted from the USCS Genome Browser primate genomic alignments. Only great apes exhibit a stable hairpin structure characteristic of miRNA precursors. Consistent with the notion that this miRNA is only present in great apes, no read matching the macaque orthologous sequence could be identified in our macaque RNA-seq data.

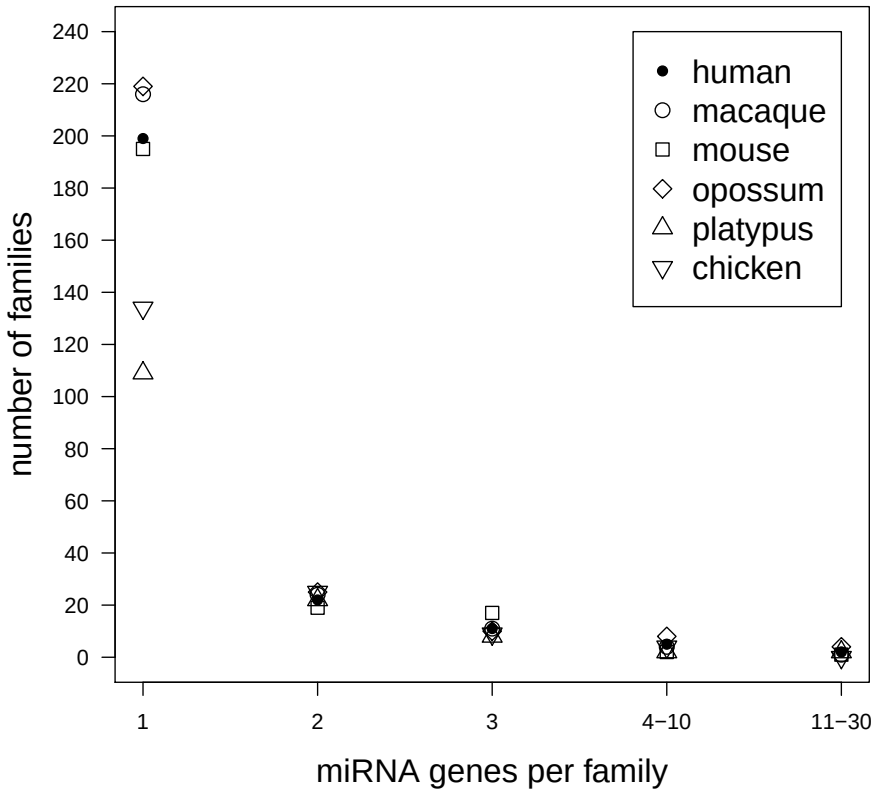

Supplementary Figure 10: Size distribution of miRNA families.

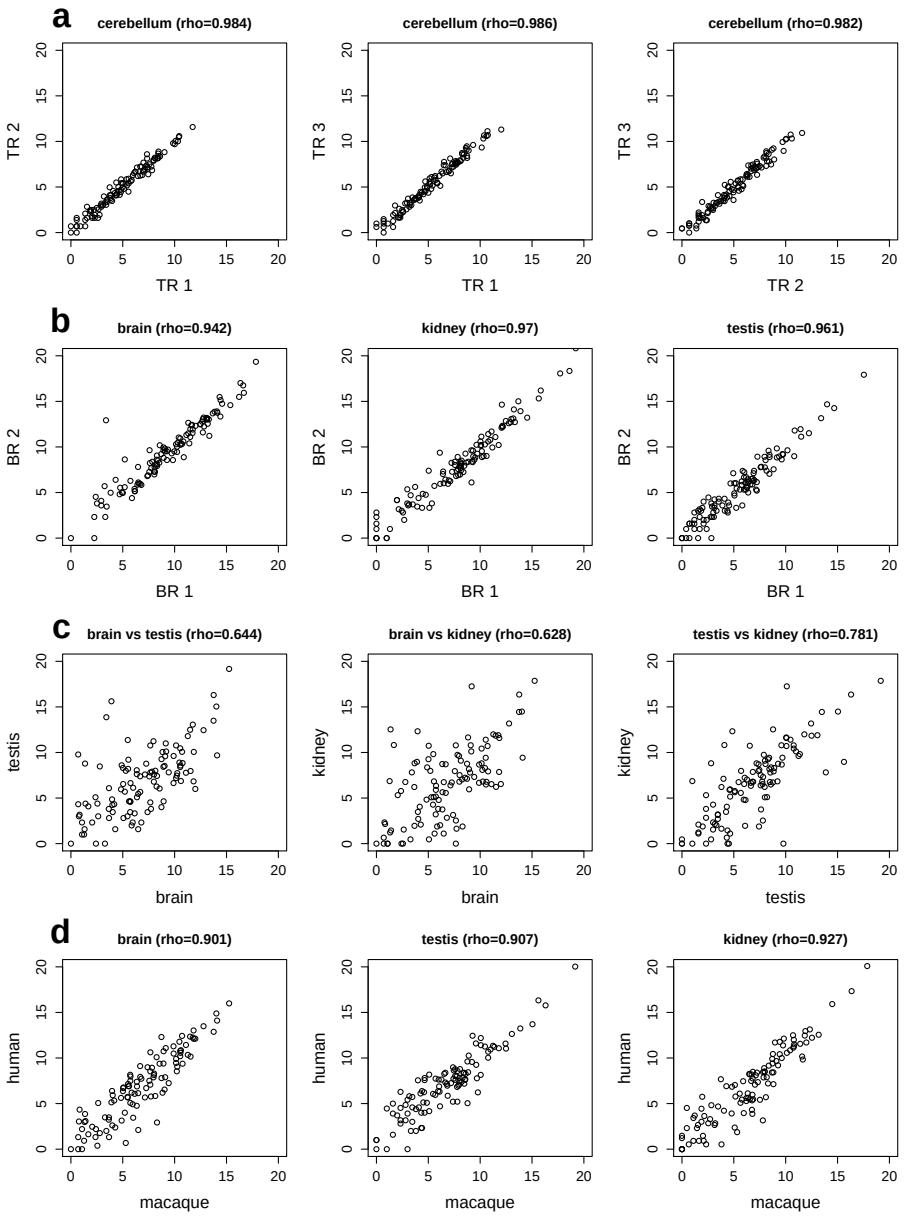

Supplementary Figure 11: Variability of miRNA expression. a-d, Correlations of expression levels (log2-transformed) for human and/or macaque 1:1 orthologous miRNA genes are shown. **a,** Correlation of macaque miRNA expression levels between technical replicates (TR). **b,** Correlation of macaque miRNA expression levels between biological replicates (BR). We note that correlation coefficients for opossum biological replicates were similar (rho: 0.972-0.975). **c,** Correlation of macaque miRNA expression levels between tissues. **d,** Correlation of miRNA expression levels between human and macaque orthologs.

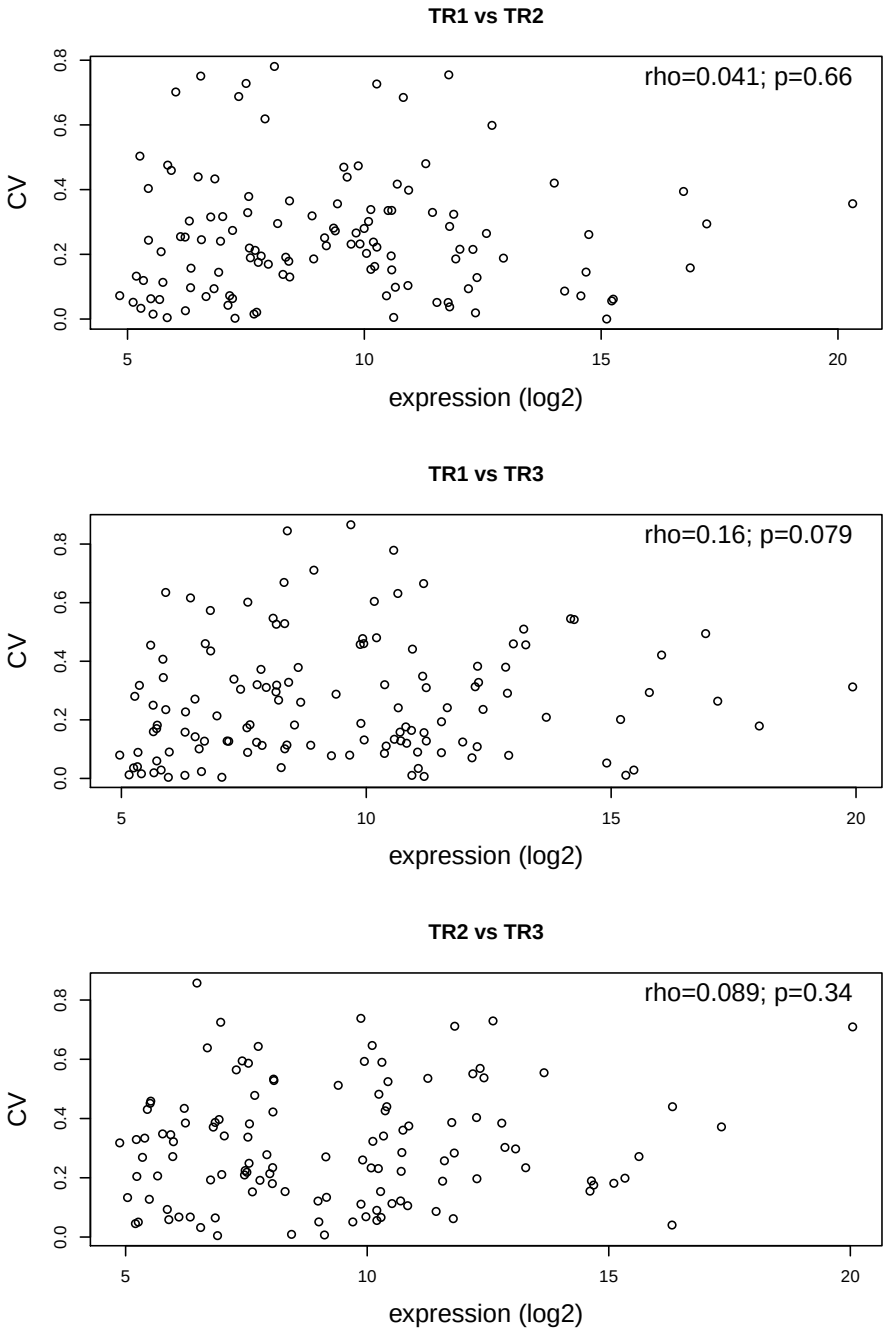

Supplementary Figure 12: Expression levels of miRNA families and technical noise. Correlation between expression levels and expression variability (CV) of technical replicates (TR) in the macaque cerebellum. CV: Coefficient of Variation (sd/mean) of expression values between two technical replicates. Expression levels were measured in each miRNA family by summing expression levels of individual miRNA genes, excluding families with less than 30 reads in total. The mean expression level (log2-transformed) in the two replicates is represented on the X-axis.

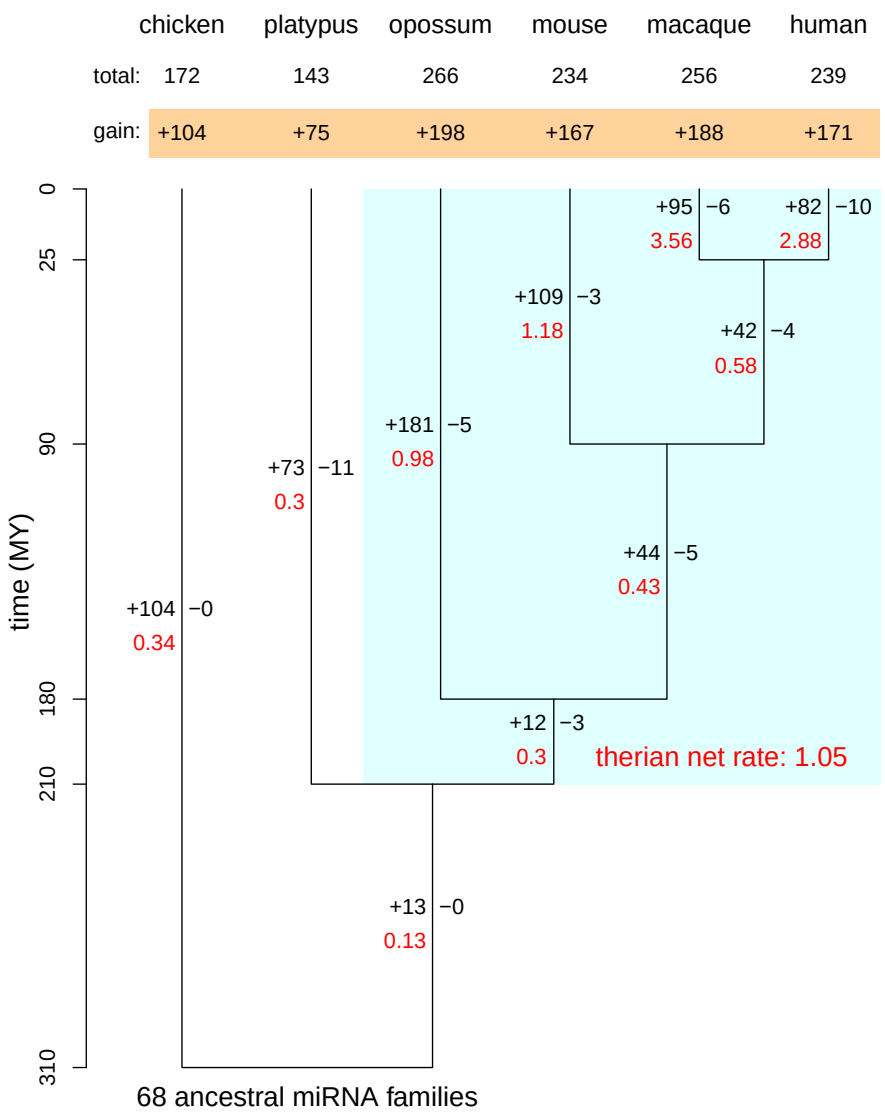

Supplementary Figure 13: Birth and death rates of miRNA families. Phylogeny of the six studied amniote species and estimated rates of miRNA family gain and loss, as inferred by Wagner parsimony (gain penalty parameter values between 0.7 and 1), are shown. Branch lengths reflect evolutionary divergence times (million of years, MY). Number of gained (+) and lost (−) families (in black) as well as the net gain rate of miRNA families per million years (in red) are indicated next to each branch. The therian net gain rate was computed based on the gain and loss of miRNA families across the entire therian clade (light blue box). The net number of families that have been gained since the bird-mammal split are indicated in the orange box and the total number of families in our dataset for each species are indicated above.

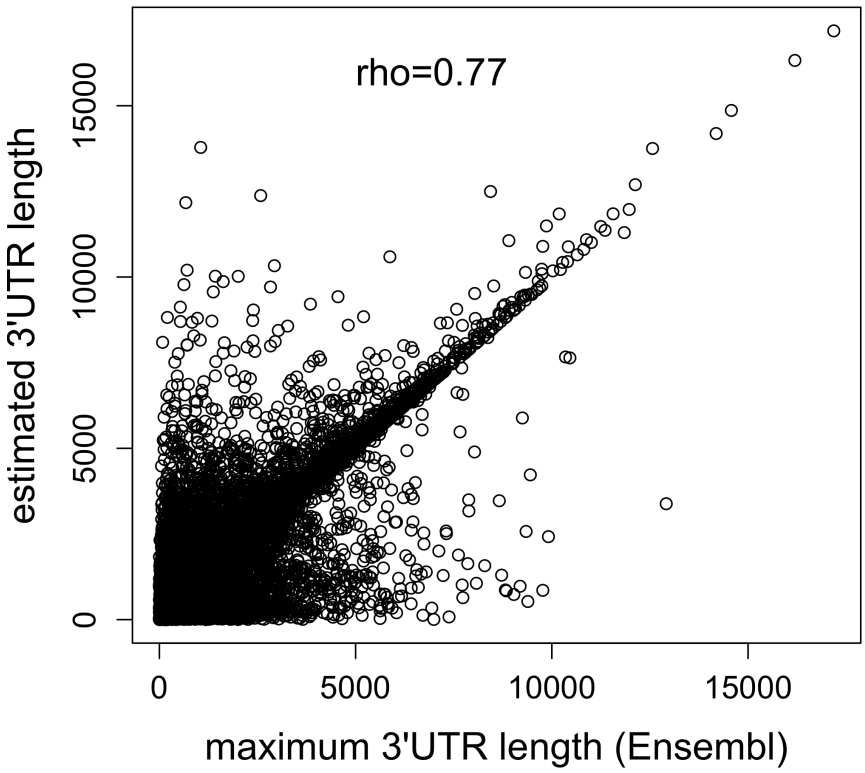

Supplementary Figure 14: Correlation between the estimated 3'UTR length of human protein-coding gene (as described in Methods) and the maximum 3'UTR length of Ensembl transcripts (Release 63).

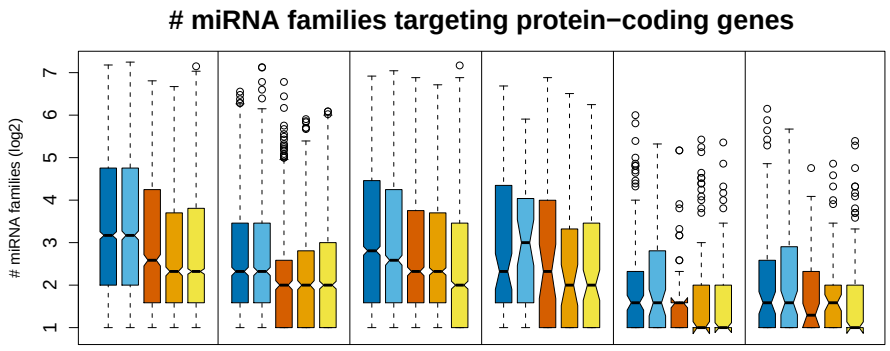

Supplementary Figure 15: Number of miRNA families targeting protein-coding genes, using TargetScan predictions. A miRNA family was considered to target a gene if one or more of the miRNAs were predicted to target the gene's 3'UTR (Methods).